PHYSICAL REVIEW B **87**, 184403 (2013)

Field-induced internal Fe and Ln spin reorientation in butterfly $\{Fe_3LnO_2\}$ (Ln = Dy and Gd) single-molecule magnets

L. Badía-Romano,* F. Bartolomé, and J. Bartolomé
Instituto de Ciencia de Materiales de Aragón (ICMA), Departamento de Física de la Materia Condensada, CSIC—Universidad de Zaragoza, E-50009 Zaragoza, Spain

J. Luzón
Instituto de Ciencia de Materiales de Aragón (ICMA), CSIC—Universidad de Zaragoza, E-50009 Zaragoza, and Academia General Militar, Centro Universitario de la Defensa, E-50015 Zaragoza, Spain

D. Prodius, C. Turta, and V. Mereacre
Institute of Chemistry, Academy of Sciences of Moldova, MD-2028 Chisinau, Republic of Moldova

F. Wilhelm and A. Rogalev
European Synchrotron Radiation Facility (ESRF), F-38043 Grenoble, France

(Received 12 December 2012; published 6 May 2013)

The intramolecular exchange interactions within the single-molecule magnet (SMM) "butterfly" molecule $[Fe_3Ln(\mu_3\text{-}O)_2(CCl_3COO)_8(H_2O)(THF)_3]$, where Ln(III) represents a lanthanide cation, are determined in a combined experimental [x-ray magnetic circular dichroism (XMCD) and vibrating sample magnetometer (VSM)] and theoretical work. Compounds with Ln = Gd and Dy, which represent extreme cases where the rare earth presents single-ion isotropic and uniaxial anisotropy, on one hand, and with Ln = Lu and Y(III) as pseudolanthanide substitutions that supply a nonmagnetic Ln reference case, on the other hand, are studied. The Dy single-ion uniaxial anisotropy is estimated from *ab initio* calculations. Low-temperature ($T \simeq 2.5$ K) hard x-ray XMCD at the Ln $L_{2,3}$ edges and VSM measurements as a function of the field indicate that the Ln moment dominates the polarization of the molecule by the applied field. Within the $\{Fe_3LnO_2\}$ cluster the Ln-Fe_3 subcluster interaction is determined to be antiferromagnetic in both Dy and Gd compounds, with values $J_{Dy\text{-}Fe_3} = -0.4$ K and $J_{Gd\text{-}Fe_3} = -0.25$ K, by fitting to spin Hamiltonian simulations that consider the competing effects of intracluster interactions and the external applied magnetic field. In the uniaxial anisotropic $\{Fe_3DyO_2\}$ case, a field-induced reorientation of the Fe_3 and Dy spins from an antiparallel to a parallel orientation takes place at a threshold field ($\mu_0 H = 4$ T). In contrast, in isotropic $\{Fe_3GdO_2\}$ this reorientation does not occur.

DOI: 10.1103/PhysRevB.87.184403 PACS number(s): 75.50.Xx, 75.10.Dg, 75.30.Et, 75.30.Gw

I. INTRODUCTION

The search for new polynuclear coordination compounds, which behave as a single-molecule magnet (SMM) has attracted special attention in the past decade, due to the possibility of using them as magnetic storage or quantum computing elements.[1–5] In addition, they provide a variety of new chemical and physical properties, such as the possibility of chemically inducing magnetic anisotropy and of exploiting intramolecular exchange interactions. Indeed, a number of lanthanide-based complexes showing SMM behavior have been reported.[6–9]

The synthesis of molecules combining the magnetic moment and relatively strong exchange interactions of 3*d* transition metals (M) with the anisotropy naturally provided by lanthanide (Ln) ions is especially promising. Several molecular clusters of this type have been reported, such as $\{Mn_4Ln_4\}$,[10] $\{Mn_{12}Gd\}$,[11] and $\{Cr_4Dy_4\}$,[12] with Ln = heavy Ln's, and $\{Mn_{11}Ln_2\}$,[13,14] with Ln = light rare earths. It was found that, in particular, Dy(III) ions are very useful for introducing anisotropy into these molecules,[15] thus confirming the possibility of achieving increased anisotropy in the lanthanide–transition-metal molecular combination. This path has also been successful in developing new SMM systems with Dy-Fe clusters, such as a complex with the planar $\{Fe_2Dy_2\}$ core.[16–19]

Though the intracluster Ln-M interaction governs the magnetic properties of this type of SMM, its nature is not entirely understood. We aim in this work to characterize its strength and anisotropy in two compounds in the series $[Fe_3Ln(\mu_3\text{-}O)_2(CCl_3COO)_8(H_2O)(THF)_3]$ (henceforth denoted $\{Fe_3LnO_2\}$ here), which also show SMM behavior, when synthesized both with nonmagnetic lanthanides, such as Lu and the pseudolanthanide Y(III), and with magnetic Ln = Gd, Tb, Dy, and Ho.[20]

SMM compounds, such as the Mn_{12} acetate cluster[21–28] and the Fe_8 cluster,[29–31] have been exhaustively studied using the giant spin model. This model is based on a strong exchange approximation which consists of considering only the total spin of the molecule, i.e., coupling the spins of all the magnetic atoms of the core. In this way, under an applied field only the total spin magnetization and the magnetic properties of the total molecule can be determined.

However, the application of nuclear-sensitive probes (neutron diffraction, Mössbauer spectroscopy, and NMR) or element-specific spectroscopies [x-ray circular magnetic dichroism (XMCD), among others] has started to provide

relevant results beyond the limitations of the previous approach: these techniques provide information about the microscopic disposition of magnetic moments and the mechanisms of relative spin orientation within the molecule. The XMCD element-selective technique has been successfully used to study the relative orientations of the different magnetic sublattices, for example, on bulk $Nd_2Fe_{14}B$ intermetallic compounds.[32] More recently, in SMM powders, the ferromagnetic coupling of the rare earth and the transition metal in the tetranuclear $[MLLn(hfac)_2]_2$, with M = Cu and Ni and Ln = Dy and Tb, was shown to occur with XMCD performed on the $L_{2,3}$ of the transition metal and the $M_{4,5}$ edges of the Ln.[33] The isostructural series of dinuclear Dy(III)-Cr(III) clusters has been characterized by means of XMCD and SQUID magnetometry. The combination of these techniques has revealed a weak antiferromagnetic (AF) Dy(III)-Cr(III) coupling.[34] Moreover, in a trimer Dy-Cr-Dy compound the transition from an antiparallel to a parallel orientation of the Cr moment with respect to that of Dy for an increasing field could be shown to occur by the same technique.[35]

In the case of molecules adsorbed on metallic surfaces the XMCD technique is extremely useful since, besides being element selective, it has submonolayer sensitivity. For example, the occurrence of quantum magnetic tunneling[2] has been proven by performing XMCD at the Fe $L_{2,3}$ edges on Fe_4 tripod cluster molecules deposited on Au substrates. The XMCD measured at the Fe and Cr $L_{2,3}$ edges on Fe_3Cr tripod clusters, with a central Cr atom, deposited on Au showed that the antiparallel alignment between Fe and Cr spins is preserved on surfaces.[36] Cr_7Ni ring spin clusters assembled on a Au substrate have also been investigated using XMCD technique as a function of temperature and field, demonstrating that the relative orientation between the Cr and the Ni magnetic moments changes from antiparallel to parallel with increasing temperature.[37] In addition, SMM behavior has also been proven in the endohedral system $DySc_2N@C_{80}$ with complementary XMCD and SQUID measurements.[38]

The effect of ligand substitution on the interaction between the Dy ions and the Fe ions on $\{Fe_2Dy_2\}$ clusters has been investigated by means of Mössbauer spectroscopy.[39] The results indicate that the Dy(III)-Fe(III) interactions and shape anisotropy are controlled by a combination of the ligand-field (LF) interaction and the applied magnetic field.

Mössbauer studies have been systematically performed on the $\{Fe_3LnO_2\}$ series of tetranuclear compounds, where Ln(III) represents the lanthanide cations (Lu, Gd, Tb, Dy, and Ho) or Y(III) as a pseudolanthanide. The hyperfine fields of the Fe atoms are found to vary as a function of the applied field in a different way, depending on the lanthanide anisotropy present in the compound.[20] Moreover, these Mössbauer data reveal that the three Fe ions in the $\{Fe_3YO_2\}$ cluster are antiferromagnetically coupled, i.e., forming a spin configuration with two $S = 5/2$ Fe up and one down.

The present work deals with the characterization of the magnetic behavior of the title compounds from a microscopic point of view. The main objective is to study the interaction between the Fe_3 subcluster and the Ln within the $\{Fe_3LnO_2\}$ cluster, by applying a competing external field and low temperatures to provoke the polarization of the Fe and Ln magnetization within the molecule. To carry out this purpose, we measure XMCD at the $L_{2,3}$ edges of the lanthanide ion as a function of the applied magnetic field.

The magnetic behavior of the Ln atoms is dominated by $4f$ unpaired electrons. On the other hand, at the $L_{2,3}$ edges the dominant signal corresponds to $2p \rightarrow 5d$ transitions, thus only the magnetism originating from $5d$ states is probed. However, due to the positive intra-atomic exchange coupling the spin of the $5d$ electrons aligns parallel to that of the $4f$ ones.[40] Therefore, the evolution with the field of the local magnetization from the $4f$ states is directly proportional to the amplitude of the XMCD signal at the $L_{2,3}$ edges.

A theoretical model and computer code have been developed to predict the Ln and Fe subcluster magnetization dependence on applied field and temperature separately, yielding excellent agreement with the experimental data. We focus our investigation on two compounds in the series $\{Fe_3LnO_2\}$ which possess the most extreme and opposite behaviors—i.e., Ln = Dy is the lanthanide with the highest anisotropy and Ln = Gd the most isotropic one—to directly compare the effects of the Ln anisotropy on the intramolecular spin reorientation and determine the Ln-Fe_3 interaction strength.

II. EXPERIMENTAL PROCEDURE

A. Synthesis and structure

The studied complexes are of the type $[Fe_3Ln(\mu_3\text{-}O)_2(CCl_3COO)_8(H_2O)(THF)_3]$, where Ln represents the lanthanide cations Gd and Dy. The synthesis of the compounds is briefly reviewed in Refs. 41 and 42. The structure of the $\{Fe_3DyO_2\}$ complex is shown in Fig. 1(a) as an example. The tetranuclear entity has a "butterfly"-type structure, with two $Fe_2Ln(\mu_3\text{-}O)$ triangular wings sharing a Ln-Fe body and a dihedral angle between the wings of 146.5°. Each Fe center is surrounded by six oxygen donor atoms. However, the precise donor set is different for each iron, the environments of Fe(1) and Fe(3) being closely similar, whereas the Fe(2) environment is significantly different.[20] Fe(1) and Fe(3) are located at the wing tips and are denoted Fe_w, while Fe(2), in the body, is designated Fe_b. One may consider the magnetic core formed by a triangular pyramid where the basis is an obtuse isosceles triangle with three Fe(III) located at the vertices and Ln located at the pyramid apex [Fig. 1(b)].

B. Magnetic and XMCD measurements

Both bulk magnetometries and XMCD measure the projection of a magnetization along the magnetic applied field. In the XMCD case, the relevant magnetization is that of the x-ray absorbing sublattice, which is selected by tuning the monochromator to a given energy edge. The total magnetization was measured on a randomly oriented powder mixed with daphne oil on a PPMS measurement platform with a vibrating sample magnetometer (VSM) option, at a temperature of 2.7 and 2.2 K and a field of up to 14 and 9 T for the Dy and Gd compounds, respectively. Excitation frequencies were varied within the range from 10 to 1500 Hz.

XANES and XMCD experiments were performed at the ID12 beamline of the ESRF, dedicated to polarization-dependent x-ray spectroscopy in the energy range from 2 to 20 keV.[43] This energy range covers the $L_{2,3}$ edges of Dy

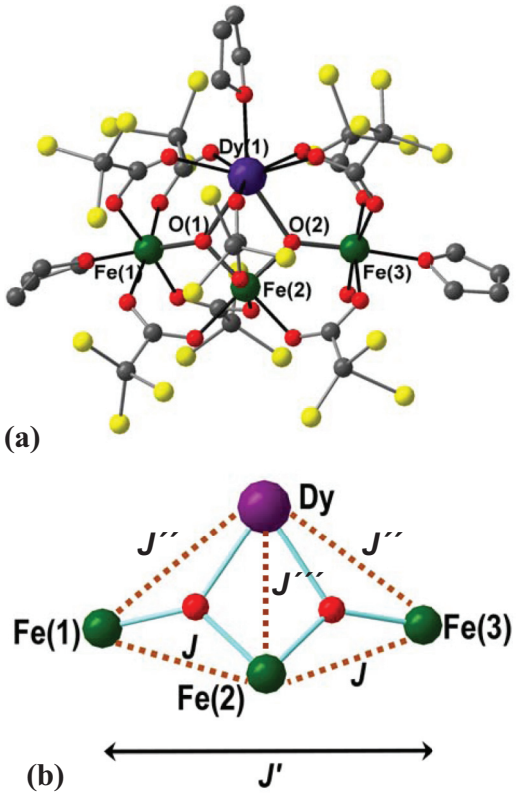

FIG. 1. (Color online) (a) Structure of Fe_3Dy complex. (b) The $\{Fe_3DyO_2\}$ core of the compound and the defined interatomic exchange parameters.

(7.8–8.6 keV) and Gd (7.2–8 keV). In these experiments circular polarized x-ray photons were generated by the second harmonic of the HU-52 Helios-II undulator. Incoming radiation was monochromatized by a double-Si(111) crystal with a polarization rate of more than 95% in all cases. XMCD signals were obtained as the direct difference of two X-ray absorption near-edge structure (XANES) spectra recorded with left and right circularly polarized x rays. The detection technique was total fluorescence yield in backscattering geometry. All measurements were performed at the low temperature of about 2.5 K. In order to minimize the radiation damage possibly affecting our samples, the brilliance of the beam incoming onto the sample was reduced by a factor of 600 compared to the x rays provided by the first harmonic of an Apple-II (typical undulator at these energies) using the second harmonic of the Helios-II helical undulator together with a set of Al and Cu attenuators. Samples were prepared as powder pellets circa 8 mm in diameter and mounted on a sample holder that could be screwed tightly on the cold finger in a liquid helium flow cryostat inserted into a 17-T superconducting magnet.

To obtain a magnetization curve from the XMCD measurements the incoming photon energy was fixed to the specific energy of the maximum XMCD amplitude. The XMCD spectra measured as a function of the applied field were recorded at a temperature of 2.7 K and a field of up to 17 T (for Ln = Dy) and $T = 2.2$ K and a field of up to 9 T (for Ln = Gd).

The Fe K-edge XMCD spectra were also recorded for the different $\{Fe_3LnO_2\}$ compounds at a temperature of 2.7 K and a magnetic field of 17 T. The Fe K-edge XMCD signal is very low since Fe(III) has a quenched total orbital moment. Indeed, for d^5 one expects $L_z = 0$ in the $3d$ states and, consequently a very low signal from excitations to the $4p$ states. In our case the signal was smaller than the experimental error.

III. THEORETICAL MODEL

A. The Fe_3 subcluster magnetic contribution

$M(H)$ and $\chi T(T)$ curves of the complexes $\{Fe_3LnO_2\}$ with Ln = Y and Lu were measured in Ref. 20. The $M(H)$ of both of them has a saturation value very close to $5\mu_B$ (Fig. 2; filled stars and filled triangles). As these two lanthanides are nonmagnetic, all the magnetic contribution in these complexes is due to the three Fe(III) which form the subcluster. In Ref. 20, the $M(H)$ and $\chi T(T)$ data on these two complexes have been interpreted by means of a model which consists of considering the three Fe atoms to form a triangle, with each Fe placed on each vertex (Fe_w, Fe_b, and Fe_w) and a certain exchange interaction acting between them (J and J') [Fig. 1(b)].

The Hamiltonian describing the Fe_3 subcluster, in the Heisenberg-Dirac-Van Vleck (HDVV) approximation, is

$$\hat{H}_{Fe_3} = -2J(\vec{S}_1 \cdot \vec{S}_2 + \vec{S}_2 \cdot \vec{S}_3) - 2J'(\vec{S}_1 \cdot \vec{S}_3). \qquad (1)$$

In this way, the $\chi T(T)$ data were fitted, leading to the conclusion that the exchange interaction $J/k_B \simeq -50$ K between both pairs of Fe_w-Fe_b is identical and AF, while the interaction J' between Fe_w-Fe_w is considered ferromagnetic and negligibly small [Fig. 1(b)]. Note that the $M(H)$ data on the two complexes, $\{Fe_3YO_2\}$ and $\{Fe_3LuO_2\}$, are well fitted with the exchange interaction values $J/k_B \simeq -50$ K and $J'/k_B = 0$ K (Fig. 2). It is important to remark that in a three-spin triangle with AF interaction, a frustration effect may be encountered if the exchange interaction between the three atoms is similar. However, no frustration happens in this case since the interaction between the Fe_w moments is negligible.

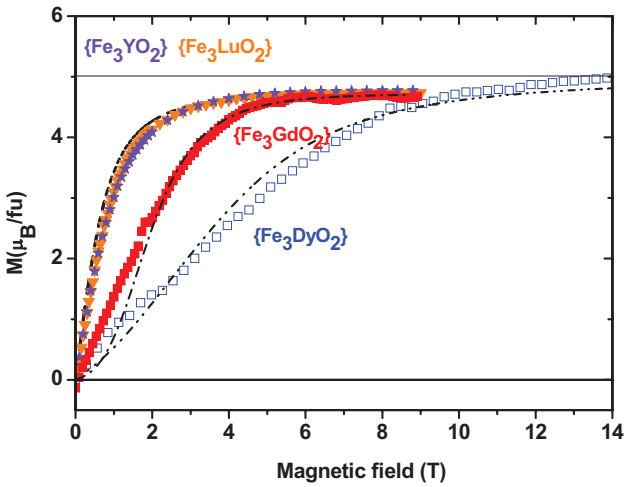

FIG. 2. (Color online) $M_{tot}(H)$ data on $\{Fe_3YO_2\}$ (filled stars) and $\{Fe_3LuO_2\}$ (filled triangles). The $M(H)$ fitted curve with $J/k_B \simeq -50$ K and $J'/k_B = 0$ (dashed line). $M_{Fe_3}(H)$ curves of $\{Fe_3DyO_2\}$ (open squares) and $\{Fe_3GdO_2\}$ (filled squares), and their corresponding simulated curves $M^{th}_{Fe_3}(H)$, for the Dy compound (dash-dot-dot line) and for the Gd compound (dash-dot line).

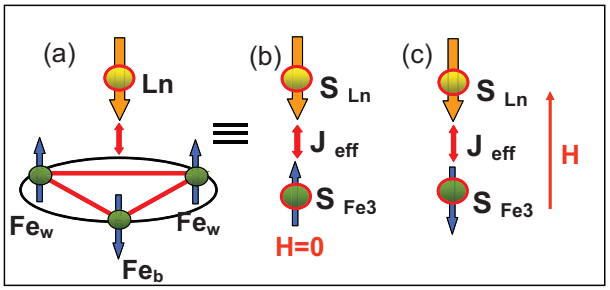

FIG. 3. (Color online) (a) Scheme of the interaction Ln-Fe_3 (double headed arrow) within the $\{Fe_3LnO_2\}$ cluster. The Fe_3 group [large (red) triangle] is substituted by a single spin S_{Fe_3}. (b) Simplified scheme of (a) at a magnetic field $H = 0$. (c) Simplified scheme of the system when a high magnetic field is applied.

The measured saturation value of 4.7 μ_B indicates that the ground state of the three Fe atoms in the cluster is that of three antiferromagnetically coupled Fe(III) $S = 5/2$ moments, leading to a total spin of the Fe_3 triangle of $S_{Fe_3} = 5/2$ [Figs. 3(a) and 3(b)]. Moreover, Mössbauer studies performed on these $\{Fe_3LnO_2\}$ complexes nicely confirm that the total Fe_3 subcluster spin is $S_{Fe_3} = 5/2$ (see Ref. 20). So, the Fe_3 triangle may be considered a robust magnetic self-unit, with effective spin $S_{Fe_3} = 5/2$ and isotropic tensor $\hat{g}_{Fe_3} = 2$ at low temperatures ($k_B T \ll J/k_B$) [Fig. 3(b)].

B. Magnetic Ln ions

The Hamiltonian including the intracluster exchange interaction and the Ln ligand-field interaction $\hat{H}_{LF}$ is

$$\hat{H}_{cluster} = \hat{H}_{Fe_3} + \hat{H}_{Ln\text{-}Fe_3} + \hat{H}_{LF}, \tag{2}$$

where

$$\begin{aligned} \hat{H}_{Ln\text{-}Fe_3} &= -2J''(\vec{S}_1 \cdot \vec{S}_{Ln} + \vec{S}_3 \cdot \vec{S}_{Ln}) \\ -2J'''(\vec{S}_2 \cdot \vec{S}_{Ln}) &= -2[J''(\vec{S}_1 + \vec{S}_3) + J'''\vec{S}_2] \cdot \vec{S}_{Ln}, \end{aligned} \tag{3}$$

J'' is the exchange interaction between both Ln-Fe(1) and Ln-Fe(3), and J''' is the interaction between Ln-Fe(2) [see Fig. 1(b)].

The quantum-mechanical behavior of the Fe_3 triangle ground state can be described by an effective spin $S_{Fe_3} = 5/2$, which allows simplification of the $\hat{H}_{Ln\text{-}Fe_3}$ Hamiltonian to

$$\hat{H}_{Ln\text{-}Fe_3} = -2\hat{J}_{eff}\vec{S}_{Fe_3} \cdot \vec{S}_{Ln} = -2J_{eff}\vec{S}_{Fe_3} \cdot \vec{J}_{Ln}, \tag{4}$$

where $\hat{J}_{eff}$ is the Ln-Fe_3 interaction, which may depend on the orbital moment. Taking into account that $\vec{S}_{Ln} = (g_J - 1)\vec{J}_{Ln}$, it can be re-expressed in terms of the effective interaction constant J_{eff} between the total angular moments $\vec{J}_{Ln}$ and $\vec{S}_{Fe_3}$ [Eq. (4), second term].

When the Hamiltonian of Eq. (3) is projected onto the Fe_3 ground state, one obtains, by equivalence with Eq. (4), $J_{eff} = 2J'' - J'''$. The eigenvalue of the Fe_3 triangle ground state is $E_0^{Fe_3}/k_B = 1250$ K, which adds as a constant in the approximation of the $\hat{H}_{cluster}$.

The ligand-field (LF) single-ion Hamiltonian may be expressed in terms of the Steven's operators O_J^M,

$$\hat{H}_{LF} = \sum_p^q B_p^q O_p^q \tag{5}$$

If the B_p^q coefficients are not known, an alternative is to determine the ligand field split electronic energy level scheme and their eigenfunctions by *ab initio* calculations.

Under an applied magnetic field, the Zeeman term $\hat{H}_z$ is added to the effective spin cluster Hamiltonian:

$$\hat{H}_{cluster} = E_0^{Fe_3} + \hat{H}_{Ln\text{-}Fe_3} + \hat{H}_{LF} + \hat{H}_z. \tag{6}$$

1. *Ln = Dy(III): Magnetic and highly anisotropic case*

The ligand-field interaction splits the $^6H_{15/2}$ Dy ground multiplet into Kramers doublets. The coordination sphere of the Dy atom consists of eight oxygen atoms. In several compounds with Dy surrounded by a similar coordination, the ground state has been found experimentally to be axially anisotropic, with $g_z \gg g_x = g_y \simeq 0$, and an energy difference from the ground doublet to the first excited doublet ranging between 60 and 80 K.[8,44] In the absence of direct determination of the ground-state g^*-tensor components, we have estimated them by means of an *ab initio* relativistic quantum chemistry method based on Post-Hartree-Fock calculations (see Supplemental Material, Sec. I).[45] The results predict that the ground state is dominated by the $|J_{Dy}, M_J\rangle = |15/2, \pm 15/2\rangle$ Kramers doublet, while the first excited state, which lies at 25 cm^{-1} (36 K), is dominated by the $|15/2, \pm 13/2\rangle$ excited doublet, although some mixture with other states may be present. The easy anisotropy axis is predicted to be parallel to the plane containing the three Fe(III) ions and at 20° with respect to the pseudosymmetry plane of the $\{Fe_3DyO_2\}$ idealized "butterfly" molecule (see Supplemental Fig. 1, Supplemental Material, Sec. I).[45] Therefore, we may assume that at the experimental temperature $T \approx 2.5$ K, only the ground-state Kramers doublet is populated, and the effective spin approximation $S^*_{Dy} = 1/2$ may be applied.

The total Hamiltonian for the Dy case is Eq. (6), where the ligand interaction $\hat{H}_{LF}$ in the Dy case can be considered a constant, one order of magnitude larger than the exchange one. Assuming a common quantization Z axis for the Dy and the Fe_3 subcluster [Supplemental Fig. 1(b), Supplemental Material, Sec. I],[45] the exchange interaction spin Hamiltonian can be expressed as

$$\hat{H}_{Dy\text{-}Fe_3} = -2J_{eff\parallel}\left[a\vec{S}^*_{Dy} \cdot \vec{S}_{Fe_3} + (1-a)S^*_{z,Dy}S_{z,Fe_3}\right]. \tag{7}$$

Here $J_{eff\parallel}$ and $J_{eff\perp}$ are the parallel and perpendicular components of the exchange interaction constant, respectively, and a is the ratio $a = J_{eff\perp}/J_{eff\parallel}$. The Zeeman term is

$$\hat{H}_z = \left(-\hat{g}^*_{Dy}\mu_B\vec{S}^*_{Dy} - \hat{g}_{Fe_3}\mu_B\vec{S}_{Fe_3}\right) \cdot \vec{H}, \tag{8}$$

where $\vec{H}$ is the applied field, $\hat{g}_{Fe_3}$ is the isotropic g tensor for the Fe_3 triangle, and $\hat{g}^*_{Dy}$ the anisotropic g^* tensor for the Dy ion in the $S^*_{Dy} = 1/2$ model.

2. *Ln = Gd(III): Magnetic and isotropic case*

Gd is an isotropic and magnetic lanthanide with a total spin value $S_{Gd} = 7/2$ and isotropic g tensor $\hat{g}_{Gd} = 2$ (free Gd ion $^8S_{7/2}$). Indeed, the ligand-field interaction splits the $^8S_{7/2}$ into Kramers doublets, the energy distance between the levels being around 0.16 K,[46] one order of magnitude smaller than the measuring temperature ($\hat{H}_{LF} \rightarrow 0$). This justifies neglecting the ligand-field splitting in the Gd case and considering the total spin $S_{Gd} = 7/2$. The Hamiltonian of Eq. (6) with $\hat{H}_{LF} \rightarrow 0$ and the same theoretical treatment as in the Dy case are used. But in this case, the general exchange Hamiltonian $\hat{H}_{Gd\text{-}Fe_3}$ becomes the isotropic Heisenberg Hamiltonian, Eq. (9), since the isotropy of Gd implies $J_{eff\parallel} = J_{eff\perp}$, and as a consequence, the ratio $a = 1$:

$$\hat{H}_{Gd\text{-}Fe_3} = -2J_{eff}(\vec{S}_{Gd} \cdot \vec{S}_{Fe_3}). \quad (9)$$

The Zeeman interaction is assumed to be isotropic and can be presented as

$$\hat{H}_z = (-\hat{g}_{Gd}\mu_B\vec{S}_{Gd} - \hat{g}_{Fe_3}\mu_B\vec{S}_{Fe_3}) \cdot \vec{H}. \quad (10)$$

The contributions to the total magnetization due to the Ln atom and the Fe_3 subcluster were simulated by full diagonalization of the Hamiltonian (see Supplemental Material, Sec. II.)[45]

The angular averaging of magnetization was performed by calculating the magnetization for different fixed field directions $[M(\theta,\varphi)]$, randomly distributed in the angular space. Then the $M(\theta,\varphi)$ results are averaged. Each direction of the applied field is defined by the colatitude (θ) and azimuth (φ) angles. With the φ angle uniformly distributed in the $[0, 2\pi]$ interval and the colatitude θ in the $[-\pi,\pi]$ interval (specifically, we use $u = \cos\theta$, which implies u uniformly distributed in the $[-1,1]$ interval). The Δu interval value is chosen so that the average $M_{th}(H)$ calculation reaches convergence within 0.1 μ_B.

The fitting procedure of the experimental $M(H)$ data with these simulations is described later.

IV. EXPERIMENTAL RESULTS

A. XANES and XMCD at a constant field

The Ln $L_{2,3}$-edge XMCD spectra measured on the $\{Fe_3LnO_2\}$ complexes at a temperature of 2.7 K and under an applied magnetic field of up to 17 T for Ln = Dy and 9 T for Ln = Gd are displayed in Fig. 4. The spectra were normalized by setting the total $L_{2,3}$-edge jump to unity.

The L_2-edge XMCD spectral profile of the two $\{Fe_3LnO_2\}$ complexes consists of a main negative peak above the edge and a smaller positive peak at higher energy. The L_3-edge XMCD spectra of the $\{Fe_3DyO_2\}$ complex consists of a negative dip followed by a main positive peak above the edge. The latter feature is of dipolar origin, while the former spectral feature has been associated with a quadrupolar transition (E2) that should be present at the L_3-edge spectra of heavy rare earths.[47,48]

The shape and position of this Dy feature are similar to those of other XMCD spectra of insulators containing Dy (Dy_2O_3).[49] Moreover, the $L_{2,3}$-edge XMCD spectra of the $\{Fe_3DyO_2\}$ and $\{Fe_3GdO_2\}$ complexes (Fig. 4) are comparable with those of the binary $DyAl_2$ and $GdAl_2$ compounds, and

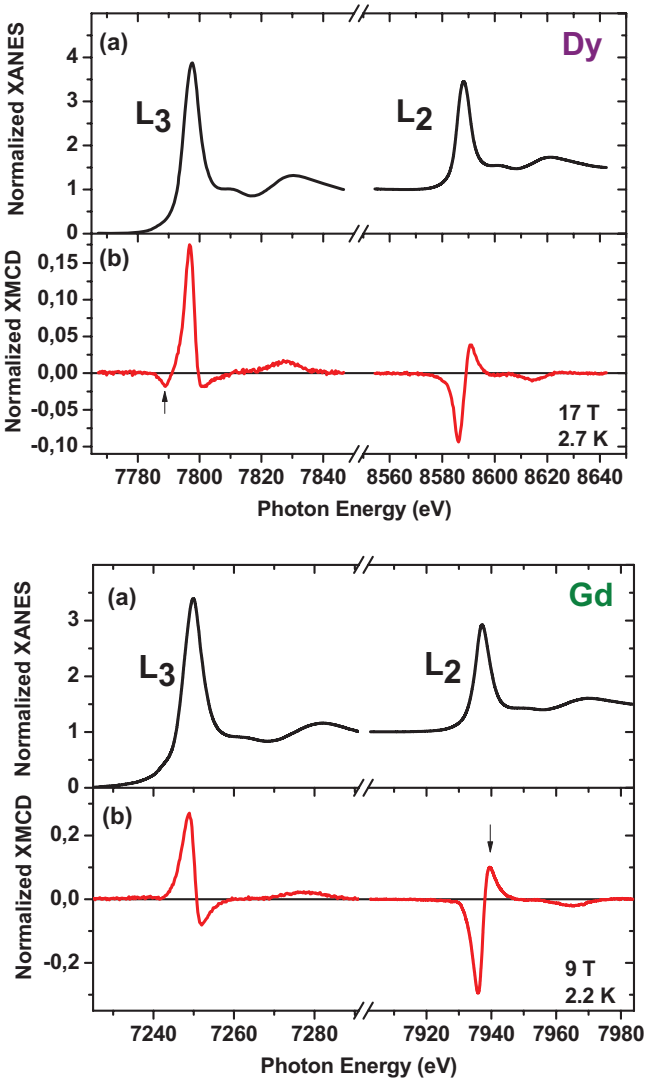

FIG. 4. (Color online) (a) XANES spectra and (b) XMCD signal at the Ln $L_{2,3}$-edges in $\{Fe_3LnO_2\}$ compounds for Ln = Dy (top) and Gd (bottom).

Al-rich $Ln(Al_{1-x}Fe_x)$ compounds (with Ln = Dy and Gd), shown in Refs. 50 and 51, respectively, which report a very similar shape and magnitude of the XMCD signal, although the latter are metallic systems. In heavy rare-earth ions the positive L_3 and negative L_2 peaks indicate that the rare-earth moment is parallel to the applied field. By comparison we may assert that the Ln moment in both compounds $\{Fe_3DyO_2\}$ and $\{Fe_3GdO_2\}$ remains parallel to the applied field at the measured temperature ($T \approx 2.5$ K) and field ($B < 9$ T). Besides, contrary to the case of Ln-Fe intermetallics,[50] no influence of Fe on the spectral shape of the Ln L edges is observed, which indicates a much weaker Ln-Fe interaction in the butterfly molecule.

The XMCD signals at the Ln $L_{2,3}$ absorption edges are affected by the contribution of quadrupolar ($2p \rightarrow 4f$) transitions[47,52–54] and by the spin dependence of the radial matrix elements of dipolar ($2p \rightarrow 5d$) transitions.[55,56] Consequently, the sum rules cannot be used to analyze the $L_{2,3}$-edge XMCD of lanthanide elements. So, the absolute spin and

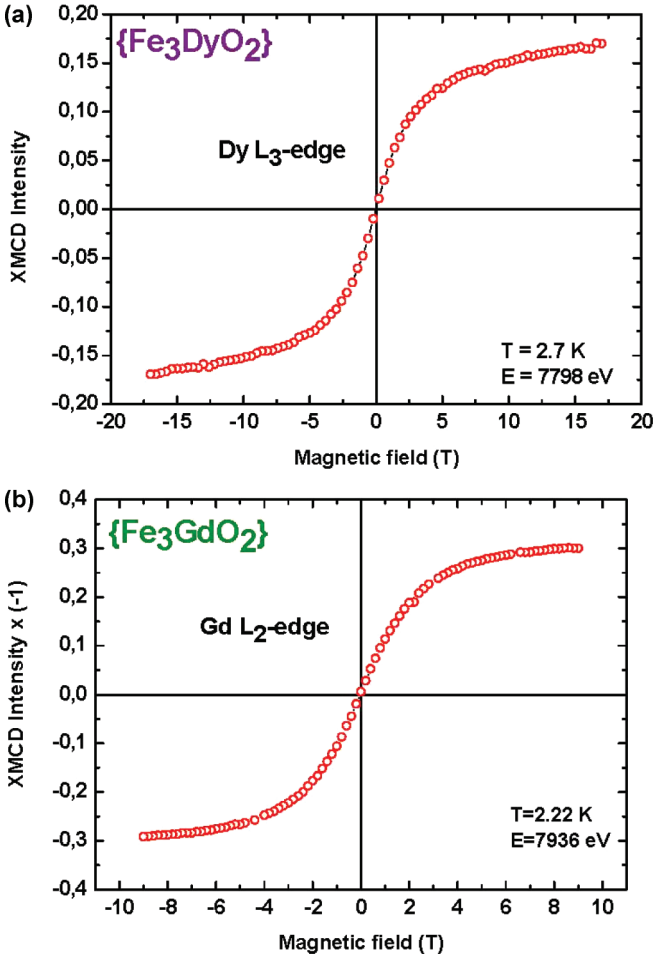

FIG. 5. (Color online) Collected magnetization curves as a function of applied field from XMCD experimental data at a fixed energy in $\{Fe_3LnO_2\}$ compounds: (a) for Ln = Dy, at $T = 2.7$ K, with the L_3 edge at $E = 7798$ eV. (b) For Ln = Gd, at $T = 2.2$ K, with the L_2 edge at $E = 7936$ eV.

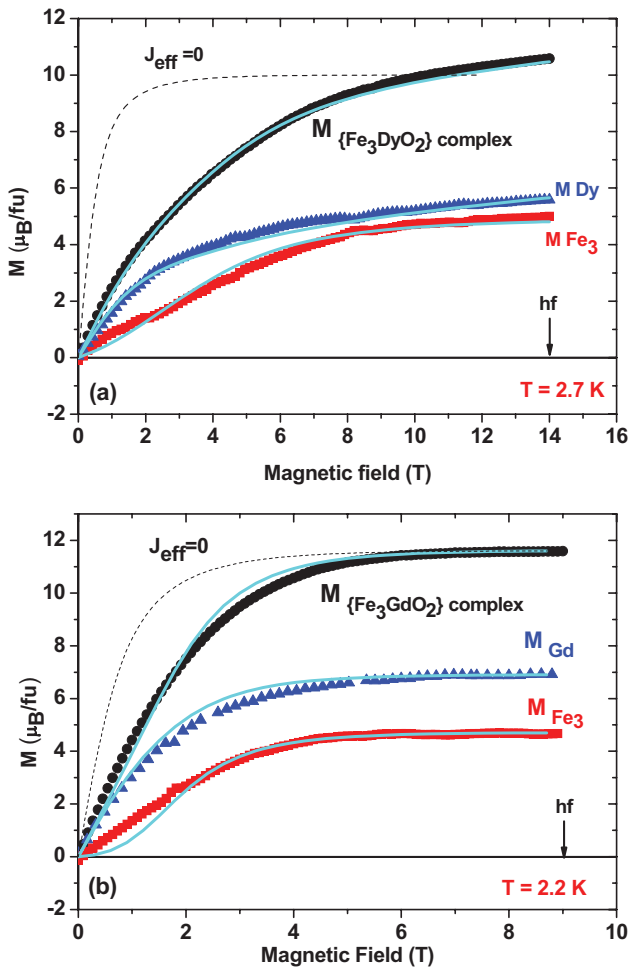

FIG. 6. (Color online) $M(H)$ curves of $\{Fe_3LnO_2\}$ compounds with (a) Ln = Dy and (b) Ln = Gd. Macroscopic $M_{tot}(H)$ curve obtained from VSM measurements at $T = 2.7$ and 2.2 K for Dy and Gd compounds, respectively (filled circles). Microscopic magnetization curve obtained by XMCD at the L_3 and L_2 edge, respectively (filled triangles). Magnetization of the total Fe present in the system obtained by subtraction of the other two curves (filled squares). $M^{th}(H)$ calculated predictions for (a) Dy and (b) Gd (solid line) at $T = 2.7$ and 2.2 K, respectively. The $M^{th}_{tot}(H)$ prediction for $J_{eff} = 0$ for (a) Dy and (b) Gd (dashed line). The black arrow indicates the high field (hf) at which the Ln magnetization curves have been scaled.

orbital moments of the Ln = Dy and Gd complexes cannot be determined experimentally from this experiment.

B. XMCD as a function of the field

The evolution with the field of the local magnetization from 4*f* states is directly proportional to the amplitude of the XMCD signal at the $L_{2,3}$ edges because of positive intra-atomic exchange interaction.[40] Magnetization curves obtained from the XMCD measurements as a function of the field, XMCD(H), at the L_3 edge of Dy (at a fixed energy $E = 7798$ eV) and L_2 edge of Gd (at energy $E = 7936$ eV), are shown in Fig. 5. These specific energies correspond to the maximum amplitude of the XMCD signal at the corresponding edge (see Fig. 4). The Gd L_3 edge is close to the Fe K-edge energy, so its XMCD could be contaminated by the Fe signal. Therefore, the Gd L_2 edge has been selected for performance of the XMCD(H) measurement. This problem does not exist in the L_3 edge of Dy.

A further point to be noted is that the Ln magnetization is parallel to the applied field at all fields, as indicated by the sign of the XMCD(H) signal for both Dy and Gd compounds. This implies that for these two compounds with a magnetic rare earth, the magnetization of the Ln subcluster dominates the total magnetization of the sample.

C. $M(H)$ measurements

The $M_{tot}(H)$ data measured with a VSM magnetometer has already been published (see Ref. 20), however, the temperature of the measurement ($T = 1.8$ K) did not coincide with the lowest temperature achieved in the XMCD experiment. Therefore, we have measured the $M_{tot}(H)$ of the $\{Fe_3DyO_2\}$ and the $\{Fe_3GdO_2\}$ compounds at $T = 2.7$ and 2.2 K, respectively, for direct comparison with the spectroscopic data. The data are depicted in Figs. 6(a) and 6(b).

TABLE I. Parameters used in the fit of all the $M(H)$ curves at low temperatures ($T = 2.7$ and 2.2 K for Dy and Gd, respectively) to the theoretical model.

Ln	S_{Ln}	g_x	g_y	g_z	$J_{eff\parallel}/k_B$ (K)	$\lvert J_{eff\perp}/k_B\rvert$ (K)	J_{eff}/k_B (K)	χ_{vv} (μ_B T^{-1}/f.u.)
Dy	1/2	0.5	2.0	17.9	−5.5(1)	3.3(1)		0.10(1)
Dy	1/2	0	0	20	−6.0(1)	4.2(1)		0.07(1)
Gd	7/2	2	2	2			−0.25(1)	

V. DISCUSSION

A. Ln and Fe_3 contributions

To study the Ln-Fe_3 interaction, the contribution to $M_{tot}(H)$ from each of the two subcluster components, Ln and Fe_3, should be separately determined from experiments at the lowest temperature measured. The magnetization contributed by the Ln ion, M_{Ln}, is determined from the XMCD(H) isothermal measurement, with the shortcoming that the absolute scale is not known. On the other hand, the total magnetization $M_{tot} = M_{Ln} + M_{Fe_3}$ performed at the same temperature, encompassing both contributions, has been determined experimentally by VSM measurements. To achieve our purpose, two steps need to be done: first, scaling the $M_{Ln}(H)$ and, second, obtaining $M_{Fe_3}(H)$.

To accomplish the first step, the VSM macroscopic $M_{tot}(H)$ measurements are analyzed at high fields. It is important to remark that the experiments were performed on randomly oriented powder samples. The randomness was guaranteed at low temperatures by freezing the powder within a hexane droplet. The total saturation magnetization has two components, $M_{tot} = M_{Ln} + M_{Fe_3}$, when the applied field polarizes completely the Fe_3 sublattice and the Ln moments. Indeed, the experimental $M_{tot}(H)$ curves [see Figs. 6(a) and 6(b)] tend to saturation at high fields. In the previous section the saturation magnetization of $\{Fe_3YO_2\}$ was found to be $M^s_{Fe_3} = 4.70(5)$ μ_B (Fig. 2; filled stars). In the $\{Fe_3DyO_2\}$ case, at $T = 2.7$ K and $\mu_0 H_{hf} = 14$ T, $M^{hf}_{tot} = 10.6(1)$ μ_B [Fig. 6(a)], thus $M^{hf}_{Dy} = 5.9(2)$ μ_B. This value is very close to the expected saturation magnetization of an uniaxial anisotropic randomly oriented Dy, $M^s_{Dy} = 5$ μ_B. Indeed, the magnetic moment of Dy, when completely oriented, is $\mu = 4/3 \times 15/2 = 10$ μ_B. For a randomly oriented powder $M^s_{Dy} = 1/2\mu = 5$ μ_B. The difference may be ascribed to a van Vleck contribution, as we show later. For $\{Fe_3GdO_2\}$, at $T = 2.2$ K and $\mu_0 H_{hf} = 9$ T, $M^{hf}_{tot} = 11.6(1)$ μ_B, and consequently, the value $M^{hf}_{Gd} = 6.9(1)$ μ_B is obtained. This value coincides excellently with the saturation value of free Gd ($M^s_{free\,Gd} = \mu_B g_J S_{Gd} = 7$ μ_B).

Now the scaling factor β, where $\beta = M^{hf}_{Ln}/\mathrm{XMCD}(H_{hf})$, for both Ln substitutions can be calculated using M^{hf}_{Dy} and M^{hf}_{Gd} obtained above. The factors $\beta = 34$ and $\beta = -23$ μ_B/(normalized XMCD unit) are obtained for $\{Fe_3DyO_2\}$ and $\{Fe_3GdO_2\}$, respectively. With these two values the magnetization curve of each Ln, $M_{Ln}(H)$, is obtained for Dy and Gd, respectively [Figs. 6(a) and 6(b)], as $M_{Ln}(H) = \beta \times \mathrm{XMCD}(H)$, where XMCD($H$) data are shown in Fig. 5. By applying this methodology we may consider the factor β as a fixed parameter in each compound.

In the second step, the magnetization curve of the Fe_3 subcluster as a function of the field, $M_{Fe_3}(H)$, can be calculated as $M_{Fe_3}(H) = M_{tot}(H) - M_{Ln}(H)$ at each field [Figs. 6(a) and 6(b), filled squares]. The $M_{Fe_3}(H)$ data obtained for the two compounds are collected in Fig. 2 together with the data for the $\{Fe_3YO_2\}$ and $\{Fe_3LuO_2\}$ cases. It is qualitatively demonstrated in Fig. 2 that the effect of substituting the nonmagnetic Lu or Y with Gd or Dy is a decrease in the polarizability of the Fe_3 subcluster magnetization with the $\{Fe_3(Y,Lu)O_2\} > \{Fe_3GdO_2\} > \{Fe_3DyO_2\}$, because of the compensating effect of an intracluster Ln-Fe_3 AF coupling and an additional high anisotropy in the latter case.

B. Comparison to theoretical simulations

To demonstrate the qualitative difference between the $M_{exp}(H)$ curves and the $M^{th}_{tot}(H)$ expected in the case where there are no Ln-Fe_3 interactions, we have depicted in Figs. 6(a) and 6(b) the prediction for $J_{eff} = 0$ (dashed curves). As could be expected, $M^{th}_{tot}(H)$ in this particular case tends to collapse with the experimental results at the highest fields, demonstrating that the Fe_3 cluster and Ln magnetic moments are fully aligned at high fields. On the contrary, at lower fields $M_{exp}(H)$ is much lower than $M^{th}_{tot}(H)$ in the absence of intracluster Ln-Fe_3 coupling. This qualitatively indicates that the overall J_{eff} is AF in both $\{Fe_3DyO_2\}$ and $\{Fe_3GdO_2\}$ clusters.

We focus our attention on the $\{Fe_3DyO_2\}$ case. The two experimental contributions $M_{Fe_3}(H)$ and $M_{Dy}(H)$ independently and, obviously, the total $M_{tot}(H)$ are nicely reproduced by the theoretical model simulations calculated with the parameters listed in Table I. A linear van Vleck contribution $M_{vv}(H) = \chi_{vv}H$ has to be added to account for the linear increase observable in the high-field $M_{Dy}(H)$ data. The Dy ion anisotropy is described by the g^*-tensor components calculated by the *ab initio* method (Supplemental Material, Sec. I.)[45] The exchange constants obtained from the fit are $J_{eff\parallel}/k_B = -5.5(1)$ K and $|J_{eff\perp}/k_B| = 3.3(1)$ K. The same fit quality is achieved if the anisotropy is simplified to perfect uniaxial anisotropy, $g^*_x = g^*_y = 0$, $g^*_z = 20$, since $M^s_{Dy} = 1/2 g^*_{Dy} S^*_{Dy} = 5$ μ_B in the $S^*_{Dy} = 1/2$ approximation. The exchange constants $J_{eff\parallel}/k_B = -6.0(1)$ K and $|J_{eff\perp}/k_B| = 4.2(1)$ K are found. The transverse component of the exchange interaction Hamiltonian gives the same prediction for either positive or negative sign (Table I).

The excellent fit achieved supports the model proposed in Sec. III: The extremely anisotropic Dy establishes the preferred direction upon the application of an external field, while the Fe_3 sublattice moment, acting as a unit and interacting antiferromagnetically with the Dy moment, is polarized towards the direction of the applied field. To illustrate this statement, the $\{Fe_3DyO_2\}$ energy level Zeeman splitting scheme and the

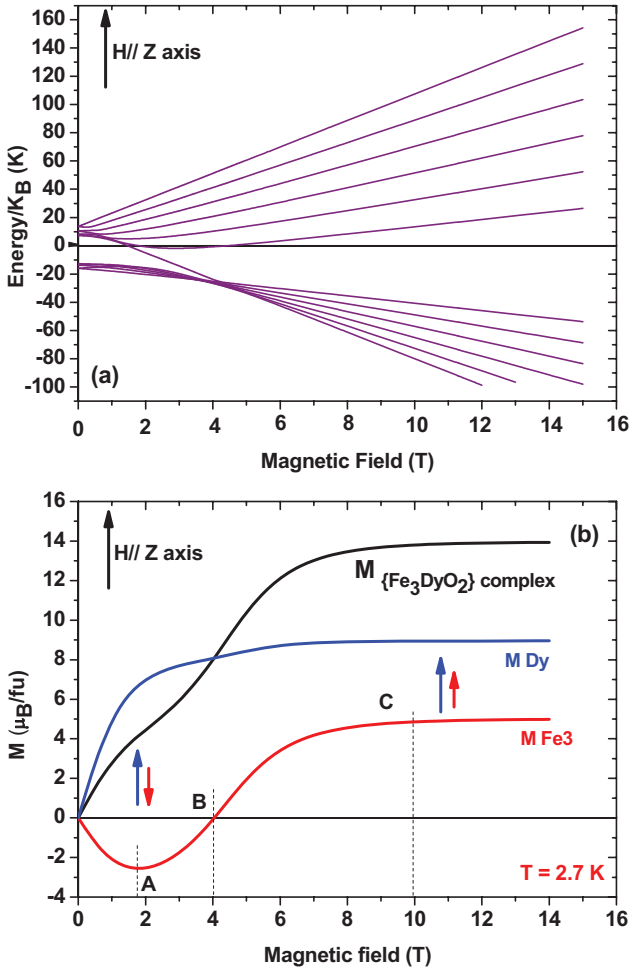

FIG. 7. (Color online) (a) Fe_3Dy energy level Zeeman splitting scheme for an applied field parallel to the Z direction (Dy EAM). (b) Simulation of the $M^{th}(H)$ curves of the $\{Fe_3DyO_2\}$ compound with $g_x^* = 0.5$, $g_y^* = 2.0$, $g_z^* = 17.9$, $J_{eff\parallel}/k_B = -5.5$ K, and $|J_{eff\perp}/k_B| = 3.3$ K. Arrows indicate the average direction of the Dy (larger arrow) and of the Fe_3 (smaller arrow) subcluster moments at point A (antiparallel) and point C (parallel); point B indicates the crossover field.

simulation of $M^{th}(H)$ for an applied field parallel to the Z direction [Dy easy axis magnetization (EAM)] are shown in Figs. 7(a) and 7(b), respectively.

At $T = 0$ the ground-state evolution with the applied field yields exact information on the expectation value of the spins in the direction of the applied field. At $T \approx 2.5$ K, the excited states also play a role since the first excited level is about 2 K above the ground state. However, the ground-state evolution still contains the dominant information to describe the evolution of the relative orientations of the Ln and the Fe_3 magnetizations, as we see below.

At $\mu_0 H = 2$ T, with a field parallel to EAM, the ground-state wave function, expressed as product wave functions, is dominated by $|S_{Fe_3}, m_{Fe_3}, S^*_{Dy}, m_{Dy}\rangle = |5/2, -5/2, 1/2, 1/2\rangle$, which indicates a probability of 97% of finding the spin configuration of the antiparallel S_{Fe_3} and S^*_{Dy} orientations. As the field increases, the wave function $|5/2, 5/2, 1/2, 1/2\rangle$, which originates from the excited multiplet at zero field, undergoes a level crossing and becomes ground state; i.e., the parallel spin configuration prevails and both the Fe_3 and the Dy spin expectation values are fully polarized in the direction of the field [Fig. 7(a)].

The thermal averaged $M_{Fe_3}(H)$ curve for an applied field along the EAM dips to negative values for fields $0 < \mu_0 H < 4.0$ T [Fig. 7(b), point A], which implies that the relative orientations of the thermally activated magnetization expected values $\langle M_{Fe_3}\rangle$ and $\langle M_{Dy}\rangle$ are antiparallel in this field domain (Supplemental Material, Sec. II.)[45] At $\mu_0 H = 4.0$ T (point B) there is a crossover to positive values, i.e., there is a reorientation of $\langle M_{Fe_3}\rangle$ from antiparallel to parallel with respect to $\langle M_{Dy}\rangle$ [point C]. When the field is applied at an angle with respect to the cluster EAM, the crossing field decreases until it becomes 0 at about 45°. This process takes place in clusters that have their EAM at an angle $\leqslant 45°$ (about 30% of clusters).

The $\{Fe_3GdO_2\}$ case is quite different since both the Fe_3 and the Gd spins have negligible anisotropy, therefore only the exchange anisotropy is acting on the spins. The fit is achieved with the isotropic $J_{eff}/k_B = -0.25$ K. The ground state evolves with the total spin $S_{tot} = 1$, for $H = 0$, to $S_{tot} = 6$ for $\mu_0 H > 3$ T. The ground state is a linear combination of wave functions (see Ref. 57) without any dominant $|S_{Fe_3}, m_{Fe_3}, S_{Gd}, m_{Gd}\rangle$ component. In conclusion, the statistical average relative orientations of Fe_3 and Gd cannot be determined until a field higher than 3 T is applied, when the ground state is dominated by the state of parallel orientations.

From this analysis it is possible to interpret the differences brought about by the two different extreme anisotropy cases in an intuitive way at the single-cluster level. Let us consider for $\{Fe_3DyO_2\}$ the simple case where the applied field and the Dy anisotropy directions are parallel. Because of the high anisotropy of Dy, single-ion anisotropy energy is dominant, and therefore it establishes the quantization direction Z, and the ground-state expectation value of the Dy moment is maximum in the direction and sign of the applied field; i.e., the applied field determines the positive direction of the Dy magnetization direction. The Dy-Fe_3 AF exchange interaction generates an internal field on the Fe_3 subcluster antiparallel to the applied field. The value of this internal field can be estimated from our fits as

$$\left|\vec{B}_{\text{Dy-Fe}_3}\right| \approx 2J_{eff}\mu_0 J_{Dy}/g_{Fe_3}\mu_B \simeq 4.5 \text{ T} \qquad (11)$$

in terms of $J_{Dy} = 15/2$, with $J_{eff}(J_{Dy} = 15/2)/k_B \approx -0.4$ K. When a nonzero field is applied in the Z direction it tends to flip the Fe_3 moment in its direction versus the opposing exchange field. The reorientation only succeeds when the applied field is larger than $|\vec{B}_{\text{Dy-Fe}_3}|$. If the applied field is at an angle with respect to the anisotropy axis, only its projection in the Z direction opposes the internal field. The described spin-field-induced spin reorientation of the Fe_3 moments is the dominant process in 30% of the molecules.

In contrast, in $\{Fe_3GdO_2\}$ there is no single-ion anisotropy field acting on Gd. As a consequence, the applied field establishes the Z quantization direction. The exchange interaction Gd-Fe_3 in this Gd case is AF, and the internal field is estimated as $|\vec{B}_{\text{Gd-Fe}_3}| < 1$ T. For this reason, the polarizability of the Fe_3 magnetization is lower than that of $\{Fe_3(Y, Lu)O_2\}$ but can never have a negative Fe_3 sublattice magnetization. Thus, the antiparallel orientation of the Fe_3 subcluster and Gd ion only

survives at $H = 0$. As soon as H is nonzero, the ground-state expectation value of the Fe_3 moment has a positive sign with respect to the applied field, so in the Gd case one cannot describe the process as spin reorientation.

The present results nicely explain the reorientation of the polarized spins within the $\{Fe_3DyO_2\}$ molecule, in the paramagnetic state under certain geometrical conditions, and the lack of reorientation in the $\{Fe_3GdO_2\}$ molecule. They let us compare the new fit parameters with those obtained in Ref. 20. In the case of the isotropic lanthanide, Gd, the g tensor is fixed at $\hat{g}_{Gd} = 2$, but the J_{eff} varies from the value $J_{eff}/k_B = -0.25$ K obtained by us to $J_{eff}/k_B = -0.35$ K,[20] which are very close to one other.

The g^*-tensor components calculated *ab initio* for Dy, $g_x^* = 0.5$, $g_y^* = 2.0$, and $g_z^* = 17.9$ yield a highly axial anisotropic character to the ground doublet. The assumption of perfectly uniaxial anisotropy ($g_x^* = g_y^* = 0, g_z^* = 20$) modifies the exchange interaction values by about 10%. Therefore, in the Dy case, this establishes exchange interaction parameter reliability. The transverse term in the anisotropic exchange Hamiltonian is justified by the fact that the real Fe_3 group is a triangle instead of a single spin, as considered in the model. The wing Dy-Fe_w interactions may provide the transverse components to the effective Hamiltonian.

In a previous Mössbauer study,[20] the polarization of the Fe spins by the external field was detected. In $\{Fe_3LuO_2\}$, Fe_w moments were found to be aligned parallel to the applied field, while Fe_b moments were aligned antiparallel. In contrast, in $\{Fe_3GdO_2\}$, only for fields higher than 2 T did the appearance of Fe hyperfine sextets announce the polarization of Fe_w spins in the field direction. $\{Fe_3DyO_2\}$ showed quite rigid Fe moments due to the magnetic anisotropy imposed by the interaction with the Dy ion. These results are in agreement with the decrease in Fe magnetization polarization with the trend $\{Fe_3LuO_2\} > \{Fe_3GdO_2\} > \{Fe_3DyO_2\}$ found in the present work.

C. Comparison to other systems

Let us compare the exchange interaction constants obtained here with those reported for other Ln-M SMMs. We denote below the $J_{Ln\text{-}M}$ interaction in terms of the real Ln spin, $J_{Dy} = 15/2$ and $S_{Gd} = 7/2$, respectively. Recently, in the dimer $[Cr(phen)_2(\mu\text{-}MeO)_2Dy\text{-}(NO_3)_4] \cdot x$MeOH ($x = 2 - 2.73$),[34] by means of XMCD measurements a very weak Dy-Cr interaction was found, $J_{Dy\text{-}Cr}/k_B = -0.06(2)$ K. Moreover, in $[Dy(hfac)_3(H_2O)\text{-}CrF_2(py)_4\text{-}Dy(hfac)_3(NO_3)]$ the transition from an antiparallel to a parallel orientation of the Cr moment with respect to the Dy one was also observed with the help of XMCD and SQUID techniques. In that case, in spite of the sample's being powdered, the negative contribution to the magnetization due to the Cr is directly observed for an applied field lower than 2 T. The Dy-Cr interaction in terms of real Dy spin ($J_{Dy} = 15/2$) was found to be $J_{Dy\text{-}Cr}/k_B = -0.25$ K. Taking into account that the Cr(III) spin is $S_{Cr} = 3/2$, a lower value with respect to the $\{Fe_3DyO_2\}$ case $J_{eff}(J_{Dy} = 15/2)/k_B = -0.4$ K, where the Fe_3(III) spin $S_{Fe_3} = 5/2$ is quite reasonable.

Just one example of Dy-Fe interaction has been studied by SQUID magnetometry and Mössbauer spectroscopy in a $[Fe_3Dy]$ dimer core molecule, and the very low antiferromagnetic interaction value $J_{Dy\text{-}Fe}/k_B = -0.1$ K (-0.07 cm^{-1}) was found,[17] which is about one-fourth of our effective interaction.

Other estimations of Gd-Fe interaction in SMM clusters have been done by SQUID magnetometry. In a "butterfly"-type $[Fe(III)_4Gd_2(\mu_4\text{-}O)_2]$ tetramer core compound two Gd-Fe interactions were distinguished: antiferromagnetic, $J_{Gd\text{-}Fe_w} = -0.17$ K (-0.12 cm^{-1}), and ferromagnetic, $J_{Gd\text{-}Fe_b} = 0.34$ K (0.24 cm^{-1}).[18] These values are similar to those found in the present Gd butterfly molecules, $J_{Gd\text{-}Fe_w} = -0.15$ and $J_{Gd\text{-}Fe_b} = 0.15$ K.[20] The triangular $[Fe_2Gd]$ trimer presents a stronger ferromagnetic Gd-Fe interaction, $J_{Gd\text{-}Fe} = 1.2(3)$ K, however, strong frustration effects take place.[58] In contrast, in a dimer, where just one Gd-Fe pathway is present, the interaction was antiferromagnetic, $J_{Gd\text{-}Fe} = -0.28$ K (-0.199 cm^{-1}).[59] From the present work, the total Gd-Fe_3 effective interaction in $\{Fe_3GdO_2\}$ is $J_{eff}/k_B = -0.25$ K.

From this review, one concludes that the Ln-Fe interaction is very weak in all cases. In future work, we expect to deepen the understanding of the magnetic evolution of the Fe_3 subcluster contribution by comparison of the calculated prediction of the Fe_3 subcluster magnetization with that obtained from the Fe $L_{2,3}$-edge and Ln $M_{4,5}$-edge XMCD experiments as a function of the applied field and at low temperatures.

VI. CONCLUSIONS

In conclusion, the element selectivity of the XMCD magnetometry together with VSM measurements have allowed us to discriminate the magnetic contributions from Ln atoms and the Fe_3 subcluster in "butterfly" clusters $\{Fe_3LnO_2\}$. With an increasing applied field the two magnetic subsystems undergo polarization in the field direction. In both Ln = Dy and Ln = Gd, M_{Ln} dominates the total magnetization.

It has been shown by *ab initio* calculations that the Dy contained in $\{Fe_3DyO_2\}$ clusters has a strong uniaxial anisotropy, as shown by the g^* tensor, $g_x^* = 0.5$, $g_y^* = 2.0$, and $g_z^* = 17.9$. However, in the case of Ln = Gd, the isotropic g tensor, $\hat{g}_{Gd} = 2$, matches the experimental data well. In the framework of an effective exchange interaction model, the Fe_3 and Ln contributions to the low-temperature magnetization as a function of the field could be fit in terms of the Ln-Fe_3 exchange interaction intensities within these SMM molecular clusters. The fits show that the Ln-Fe_3 subclusters are antiferromagnetically coupled: $J_{eff\parallel}(S_{Dy}^* = 1/2)/k_B = -5.5$ K, $|J_{eff\perp}(S_{Dy}^* = 1/2)/k_B| = 3.3$ K, and $J_{eff}(J_{Dy} = 15/2)/k_B \approx -0.4$ K for Ln = Dy and $J_{eff}/k_B = -0.25$ K for Ln = Gd.

Specifically, the experimental $M_{Fe_3}(H)$ curves of the subclusters demonstrate that the angle averaged Fe_3 subcluster contribution is always positive. The subcluster magnetization polarizability decreases with the trend $\{Fe_3(Y,Lu)O_2\} > \{Fe_3GdO_2\} > \{Fe_3DyO_2\}$ as illustrated in Fig. 2, which is due to the increasing opposition of the exchange AF field caused by the Gd ion and the additional single-ion anisotropy in the Dy. However, upon consideration in detail, one finds that about 30% of the randomly oriented $\{Fe_3DyO_2\}$ clusters in the Fe_3 subcluster moment actually change from an antiparallel to a parallel orientation with respect to the Dy moment as the field increases.

The effective interaction value in the Dy compound is AF of the order of $J_{eff}(J_{Dy} = 15/2)/k_B \approx -0.4$ K (0.28 cm^{-1}).

Such a low interaction explains why an external field larger than 4 T is capable of overcoming the exchange anisotropy and reorient the Fe_3 moment in the least favorable case (angle between easy anisotropy axis and applied field less than $<45^{\circ}$).

Besides, from this and previous work it has been deduced that the Dy-M and Gd-M interaction is very weak (of the order of several tenths of kelvins) and AF. This excludes the dipolar coupling as the main mechanism of interaction, which, for aligned clusters, would tend to polarize the moments in parallel.

One may conclude that the employment of the element selectivity of XMCD, and VSM at the molecular level has allowed us to obtain more precise information on intramolecular interactions in butterfly molecules.

ACKNOWLEDGMENTS

Discussions with J. Chaboy, P. Alonso, J. Rubín and O. Bunău are acknowledged. The financial support of Spanish MINECO Grant No. MAT2011-23791, the Alexander Von Humboldt Foundation (D.P.), and Aragonese DGA-IMANA E34 (cofunded by Fondo Social Europeo) and that received from European Union FEDER funds are also acknowledged. L.B.R. acknowledges the Spanish MINECO FPU 2010 grant. XMCD data were taken during the training period of L.B.R. carried out in ID12 at the ESRF. The authors would like to acknowledge the use of Servicio General de Apoyo a la Investigación (SAI), Universidad de Zaragoza.

*Corresponding author: lbadia@unizar.es

[1] M. Verdaguer, A. Bleuzen, C. Train, R. Garde, F. Fabrizi de Biani, and C. Desplanches, Phil. Trans. R. Soc. Lond. A **357**, 2959 (1999).
[2] M. Mannini, F. Pineider, C. Danieli, F. Totti, L. Sorace, P. Sainctavit, M. A. Arrio, E. Otero, L. Joly, J. C. Cezar, A. Cornia, and R. Sessoli, Nature **468**, 417 (2010).
[3] M. N. Leuenberger and D. Loss, Nature **410**, 789 (2001).
[4] J. Tang, I. Hewitt, N. T. Madhu, G. Chastanet, W. Wernsdorfer, C. E. Anson, C. Benelli, R. Sessoli, and A. K. Powell, Angew. Chem. Int. Ed. **45**, 1729 (2006).
[5] J. Luzon, K. Bernot, I. J. Hewitt, C. E. Anson, A. K. Powell, and R. Sessoli, Phys. Rev. Lett. **100**, 247205 (2008).
[6] N. Ishikawa, M. Sugita, T. Ishikawa, S. Koshihara, and Y. Kaizu, J. Am. Chem. Soc. **125**, 8694 (2003).
[7] X. L. Wang, L. C. Li, and D. Z. Liao, Inorg. Chem. **49**, 4735 (2010).
[8] S. D. Jiang, B. W. Wang, G. Su, Z. M. Wang, and S. Gao, Angew. Chem. Int. Ed. **49**, 7448 (2010).
[9] R. Sessoli and A. K. Powell, Coord. Chem. Rev. **259**, 2328 (2009).
[10] G. Karotsis, S. Kennedy, S. J. Teat, C. M. Beavers, D. A. Fowler, J. J. Morales, M. Evangelisti, S. J. Dalgarno, and E. K. Brechin, J. Am. Chem. Soc. **132**, 12983 (2010).
[11] T. C. Stamatatos, S. J. Teat, W. Wernsdorfer, and G. Christou, Angew. Chem. Int. Ed. **48**, 521 (2009).
[12] J. Rink, G. Novitchi, W. V. Heuvel, L. Ungur, Y. Lan, W. Wernsdorfer, C. E. Anson, L. F. Chibotaru, and A. K. Powell, Angew. Chem. Int. Ed. **49**, 7583 (2010).
[13] V. Mereacre, A. M. Ako, R. Clérac, W. Wernsdorfer, G. Filoti, J. Bartolomé, C. E. Anson, and A. K. Powell, J. Am. Chem. Soc. **129**, 9246 (2007).
[14] V. Mereacre, Y. Lan, R. Clérac, A. M. Ako, W. Wernsdorfer, G. Buth, C. Anson, and A. K. Powell, Inorg. Chem. **50**, 12001 (2011).
[15] V. Mereacre, A. M. Ako, R. Clérac, W. Wernsdorfer, I. J. Hewitt, C. E. Anson, and A. K. Powell, Chem. A Eur. J. **14**, 3577 (2008).
[16] M. Murugesu, A. Mishra, W. Wernsdorfer, K. A. Abboud, and G. Christou, Polyhedron **25**, 613 (2006).
[17] M. Ferbinteanu, T. Kajiwara, K.-Y. Choi, H. Nojiri, A. Nakamoto, N. Kojima, F. Cimpoesu, Y. Fujimura, S. Takaishi, and M. Yamashita, J. Am. Chem. Soc. **128**, 9008 (2006).
[18] M. N. Akhtar, V. Mereacre, G. Novitchi, J.-P. Tuchagues, C. E. Anson, and A. K. Powell, Chem. Eur. J. **15**, 7278 (2009).
[19] Q. Zhou, F. Yang, D. Liu, Y. Peng, G. Li, Z. Shi, and S. Fenga, Dalton Trans. **42**, 1039 (2013).
[20] J. Bartolomé, G. Filoti, V. Kuncser, G. Schinteie, V. Mereacre, C. E. Anson, A. K. Powell, D. Prodius, and C. Turta, Phys. Rev. B **80**, 014430 (2009).
[21] T. Lis, Acta Crystallogr. Sec. B **36**, 2042 (1980).
[22] A. Caneschi, D. Gatteschi, R. Sessoli, A. L. Barra, L. C. Brunel, and M. Guillot, J. Am. Chem. Soc. **113**, 5873 (1991).
[23] M. A. Novak and R. Sessoli, in *Quantum Tunnelling of Magnetization—QTM'94*, Nato ASI Series, edited by L. Gunther and B. Barbara (NATO, Brussels, 1995), pp. 171–188.
[24] R. Sessoli, H.-L. Tsai, A. R. Schake, S. Wang, J. B. Vincent, K. Folting, D. Gatteschi, G. Christou, and D. N. Hendrickson, J. Am. Chem. Soc. **115**, 1804 (1993).
[25] R. Sessoli, D. Gatteschi, A. Caneschi, and M. A. Novak, Nature **365**, 141 (1993).
[26] L. Thomas, F. Lionti, R. Ballou, D. Gatteschi, R. Sessoli, and B. Barbara, Nature **383**, 145 (1996).
[27] J. R. Friedman, M. P. Sarachik, J. Tejada, and R. Ziolo, Phys. Rev. Lett. **76**, 3830 (1996).
[28] J. M. Hernández, X. X. Zhang, F. Luis, J. Bartolomé, J. Tejada, and R. Ziolo, Europhys. Lett. **35**, 301 (1996).
[29] K. Wieghardt, K. Pohl, I. Jibril, and G. Huttner, Angew. Chem. Int. Ed. **23**, 77 (1984).
[30] A.-L. Barra, P. Debrunner, D. Gatteschi, C. E. Schulz, and R. Sessoli, Europhys. Lett. **35**, 133 (1996).
[31] L. Cianchi, F. Del Giallo, G. Spina, W. Reiff, and A. Caneschi, Phys. Rev. B **65**, 064415 (2002).
[32] J. Chaboy, A. Marcelli, L. M. García, J. Bartolomé, M. Kuzmin, H. Maruyama, K. Kobayashi, H. Kawata, and T. Iwazumi, Europhys. Lett. **28**, 135 (1994).
[33] T. Hamamatsu, K. Yabe, M. Towatari, S. Osa, N. Matsumoto, N. Re, A. Pochaba, J. Mrozinski, J.-L. Gallani, A. Barla, P. Imperia, C. Paulsen, and J.-P. Kappler, Inorg. Chem. **46**, 4458 (2007).
[34] J. Dreiser, K. S. Pedersen, T. Birk, M. Schau-Magnussen, C. Piamonteze, S. Rusponi, T. Weyhermüller, H. Brune, F. Nolting, and J. Bendix, J. Phys. Chem. A **116**, 7842 (2012).
[35] J. Dreiser, K. Pedersen, C. Piamonteze, S. Rusponi, Z. Salman, M. Ehesan-Ali, M. Schau-Magnussen, C. Thuesen, S. Piligkos, H. Weihe, H. Mutka, O. Waldmann, P. Oppeneer, J. Bendix, F. Noltinga, and H. Brunec, Chem. Sci. **3**, 1024 (2012).
[36] M. Mannini, E. Tancini, L. Sorace, P. Sainctavit, M. A. Arrio, Y. Qian, E. Otero, D. Chiappe, L. Margheriti, J. C. Cezar, R. Sessoli, and A. Cornia, Inorg. Chem. **50**, 2911 (2011).

[37]V. Corradini, A. Ghirri, E. Garlatti, R. Biagi, V. D. Renzi, U. Pennino, V. Bellini, S. Carretta, P. Santini, G. Timco, R. E. P. Winpenny, and M. Affronte, Adv. Funct. Mater. **22**, 3706 (2012).

[38]R. Westerstrom, J. Dreiser, C. Piamonteze, M. Muntwiler, S. Weyeneth, H. Brune, S. Rusponi, F. Nolting, A. Popov, S. Yang, L. Dunsch, and T. Greber, J. Am. Chem. Soc. **134**, 9840 (2012).

[39]V. Mereacre, A. Baniodeh, C. E. Anson, and A. K. Powell, J. Am. Chem. Soc. **133**, 15335 (2011).

[40]C. Giorgetti, E. Dartyge, F. Baudelet, and R.-M. Galéra, Phys. Rev. B **70**, 035105 (2004).

[41]C. Turta, D. Prodius, V. Mereacre, S. Shova, M. Gdaniec, Y. A. Simonov, V. Kuncser, G. Filoti, A. Caneschi, and L. Sorace, Inorg. Chem. Comm. **7**, 576 (2004).

[42]V. Mereacre, D. Prodius, C. Turta, S. Shova, G. Filoti, J. Bartolomé, R. Clérac, C. E. Anson, and A. K. Powell, Polyhedron **28**, 3017 (2009).

[43]A. Rogalev, J. Goulon, C. Goulon-Ginet, and C. Malgrange, in *Magnetism and Synchrotron Radiation*, Lecture Notes in Physics, Vol. 565, edited by E. Beaurepaire, F. Scheurer, G. Krill, and J. P. Kappler (Springer, Berlin, 2001), p. 60.

[44]A. Bhunia, M. T. Gamer, L. Ungur, L. F. Chibotaru, A. K. Powell, Y. Lan, P. W. Roesky, F. Menges, C. Riehn, and G. Niedner-Schatteburg, Inorg. Chem. **51**, 9589 (2012).

[45]See Supplemental Material at http://link.aps.org/supplemental/10.1103/PhysRevB.87.184403 for "*ab initio*" calculations of the Dy ground state and calculation methodology of the Ln and Fe_3 magnetization components versus magnetic field in a Ln-Fe_3 cluster.

[46]E. R. Bernstein and G. M. Dobbs, Phys. Rev. B **11**, 4623 (1975).

[47]F. Bartolomé, J. M. Tonnerre, L. Sève, D. Raoux, J. Chaboy, L. M. García, M. Krisch, and C. C. Kao, Phys. Rev. Lett. **79**, 3775 (1997).

[48]F. Bartolomé, M. H. Krisch, D. Raoux, and J.-M. Tonnerre, Phys. Rev. B **60**, 13497 (1999).

[49]C. Neumann, B. W. Hoogenboom, A. Rogalev, and J. B. Goedkoop, Solid State Commun. **110**, 375 (1999).

[50]M. A. Laguna-Marco, J. Chaboy, and C. Piquer, Phys. Rev. B **77**, 125132 (2008).

[51]M. A. Laguna-Marco, J. Chaboy, C. Piquer, H. Maruyama, N. Ishimatsu, N. Kawamura, M. Takagaki, and M. Suzuki, Phys. Rev. B **72**, 052412 (2005).

[52]J. C. Lang, S. W. Kycia, X. D. Wang, B. N. Harmon, A. I. Goldman, D. J. Branagan, R. W. McCallum, and K. D. Finkelstein, Phys. Rev. B **46**, 5298 (1992).

[53]J. C. Lang, G. Srajer, C. Detlefs, A. I. Goldman, H. König, X. Wang, B. N. Harmon, and R. W. McCallum, Phys. Rev. Lett. **74**, 4935 (1995).

[54]J. Chaboy, F. Bartolomé, L. M. García, and G. Cibin, Phys. Rev. B **57**, R5598 (1998).

[55]X. Wang, T. C. Leung, B. N. Harmon, and P. Carra, Phys. Rev. B **47**, 9087 (1993).

[56]B. N. Harmon and A. J. Freeman, Phys. Rev. B **10**, 1979 (1974).

[57]Ground-state wave function at $\mu_0 H = 1$ T in terms of $|S_{Fe_3}, m_{Fe_3}, S_{Gd}, m_{Gd}\rangle$, $\psi_0 = -0.56|5/2,-1/2,7/2,5/2\rangle + 0.53|5/2,-3/2,7/2,7/2\rangle + 0.49|5/2,1/2,7/2,3/2\rangle - 0.36|5/2,3/2,7/2,1/2\rangle + 0.2|5/2,5/2,7/2,-1/2\rangle$.

[58]S. Mukherjee, M. R. Daniels, R. Bagai, K. A. Abboud, G. Christou, and C. Lampropoulos, Polyhedron **29**, 54 (2010).

[59]M. Ferbinteanu, F. Cimpoesu, M. A. Gîrtu, C. Enachescu, and S. Tanase, Inorg. Chem. **51**, 40 (2012).